Plants in water-controlled ecosystems: active role in hydrologic processes and response to water stress
II. Probabilistic soil moisture dynamics

F. Laio [a,b], A. Porporato [a,b], L. Ridolfi [a], I. Rodriguez-Iturbe [b,*]

[a] *Dipartimento di Idraulica Trasporti e Infrastrutture Civili, Politecnico di Torino, Corso Duca degli Abruzzi, 24, 10129 Torino, Italy*
[b] *Princeton Environmental Institute and Graduate Program in Environmental Engineering and Water Resources, Princeton University, Princeton, NJ 08544, USA*

Abstract

A stochastic model for soil moisture dynamics at a point is studied in detail. Rainfall is described as a marked Poisson process, producing a state-dependent infiltration into the soil. Losses due to leakage and evapotranspiration also depend on the existing level of soil moisture through a simplifying but realistic representation of plant physiological characteristics and soil properties. The analytic solution of the steady-state probability distributions is investigated to assess the role of climate, soil, and vegetation in soil moisture dynamics and water balance. © 2001 Elsevier Science Ltd. All rights reserved.

Keywords: Soil moisture; Vegetation; Ecohydrology; Stochastic processes; Hydrology; Water stress; Water balance; Savannas; Grasslands; Crossing analysis

1. Introduction

In this paper we analyze the role of the various components of the climate–soil–vegetation system on the temporal dynamics of soil moisture. The goal is to provide a realistic description of soil moisture dynamics in an analytically tractable way, as a basis for a quantitative understanding of the vegetation response to water stress. This approach may also be useful to have insights on other processes closely related to soil moisture dynamics, such as soil–atmosphere interaction, soil production and litter decomposition, plant nutrient uptake, and soil gas emissions.

The present modeling effort constitutes an improvement and extension of the previous work by Rodriguez-Iturbe et al. [54]. We have modified their representation of evapotranspiration and leakage losses toward a more realistic description of soil moisture dynamics, especially in conditions of drought. All the various mechanisms involved and the related simplifying assumptions are discussed below with particular attention to the modeling of plant transpiration within the scheme of the soil–plant–atmosphere continuum.

2. Soil water balance at a point

Under the simplified conditions that the lateral and vertical contributions can be neglected (see Part I [55], Section 3), the soil moisture balance at a point is expressed as

$$nZ_r \frac{ds(t)}{dt} = \varphi[s(t);t] - \chi[s(t)], \qquad (1)$$

where n is the porosity; Z_r is the depth of active soil or root depth; $s(t)$ is the relative soil moisture content $(0 \leqslant s(t) \leqslant 1)$; $\varphi[s(t);t]$ is the rate of infiltration from rainfall; $\chi[s(t)]$ is the rate of soil moisture losses from the active soil.

The infiltration from rainfall, $\varphi[s(t);t]$ is the stochastic component of the balance. It represents the part of rainfall that actually reaches the soil column, i.e.,

* Corresponding author. Tel.: +1-609-258-5411; fax: +1-609-258-2799.
E-mail address: irodrigu@princeton.edu (I. Rodriguez-Iturbe).

$$\varphi[s(t); t] = R(t) - I(t) - Q[s(t); t], \qquad (2)$$

where $R(t)$ is the rainfall rate, $I(t)$ is the amount of rainfall lost through interception by canopy cover, and $Q[s(t); t]$ is the rate of runoff.

Evapotranspiration and leakage constitute the losses of the balance, i.e.,

$$\chi[s(t)] = E[s(t)] + L[s(t)], \qquad (3)$$

where $E[s(t)]$ and $L[s(t)]$ are the rates of evapotranspiration and leakage, respectively.

Eq. (1) is a stochastic, ordinary differential equation for the state variable $s(t)$. For simplicity of notation, in what follows we will dispense with the indication of the time dependence of soil moisture whenever it is not necessary. The main components of the soil–water balance described above are schematically shown in Fig. 1. We now proceed to discuss the assumptions made to model the various terms of Eq. (1). Throughout the paper it will be assumed that the model representation corresponds to a growing season in which the different climate and vegetation parameters remain constant in time. As pointed out in Part I [55], in cases where there is considerable variation in climate and vegetation parameters throughout, the growing season one possibility is to estimate two set of parameters corresponding to the early and the late growing season, respectively.
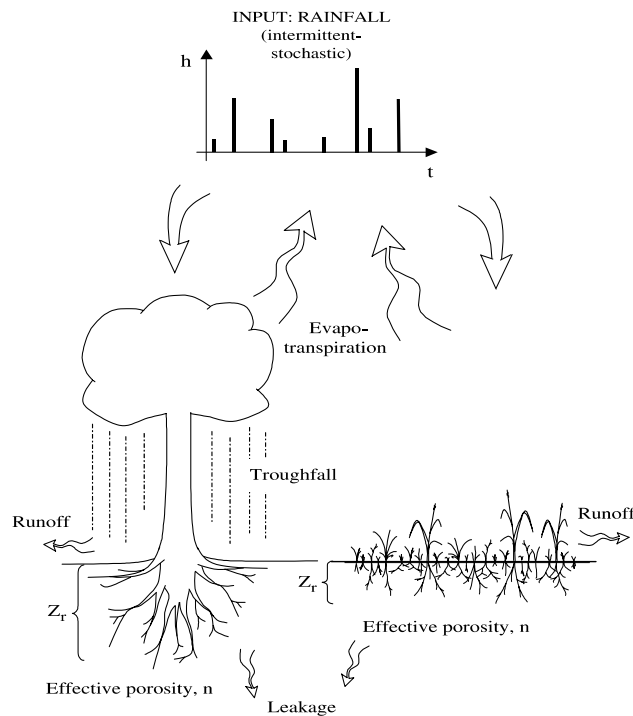

Fig. 1. Schematic representation of the various mechanisms of the soil water balance with particular emphasis on the role of different functional vegetation types.

2.1. Rainfall modeling

At small spatial scales, where the contribution to rainfall of soil-moisture recycling is negligible, the rainfall input can be treated as an external random forcing, independent of the soil moisture state. The inclusion of the stochastic nature of rainfall is essential to attempt a proper modeling of soil moisture dynamics. The response of vegetation (i.e., resistance to drought, productivity, reproduction and germination, etc.) in water-controlled ecosystems is also strongly linked to the intermittent and unpredictable character of rainfall availability (e.g., [46]).

Since the occurrence and amount of rainfall are both stochastic, we idealize the occurrence of rainfall as a series of point events in continuous time, arising in a Poisson process of rate λ and each carrying a random amount of rainfall extracted from a given distribution. The temporal structure within each rain event is ignored and the marked Poisson process representing precipitation is physically interpreted at a daily time scale, where the pulses of rainfall correspond to daily precipitation assumed to be concentrated at an instant in time.

The distribution of the times τ between precipitation events is exponential with mean $1/\lambda$ (e.g., [13]), i.e.,

$$f_{\mathrm{T}}(\tau) = \lambda e^{-\lambda \tau} \quad \text{for } \tau \geqslant 0. \qquad (4)$$

The depth of rainfall events is assumed to be an independent random variable h, described by an exponential probability density function

$$f_{\mathrm{H}}(h) = \frac{1}{\alpha} e^{-\frac{1}{\alpha} h} \quad \text{for } h \geqslant 0, \qquad (5)$$

where α is the mean depth of rainfall events. Since the model is interpreted at the daily time scale, α may be estimated as the mean daily rainfall in days when precipitation occurs. In the following we will often refer to the value of the mean rainfall depth normalized by the active soil depth, i.e.,

$$\frac{1}{\gamma} = \frac{\alpha}{n Z_{\mathrm{r}}}. \qquad (6)$$

Both distributions, Poisson and exponential, are of common use in simplified models of rainfall at daily time scale. The exponential distribution fits well daily rainfall data and, at the same time, allows analytical tractability [3,17].

Notice that the rainfall rate $R(t)$ in Eq. (2) can be linked to the probability distributions (4) and (5), if one expresses the marked Poisson process as a temporal sequence, i.e.,

$$R(t) = \sum_i h_i \delta(t - t_i), \qquad (7)$$

where $\delta(\cdot)$ is the Dirac delta function, $\{h_i, i = 1, 2, 3, \ldots\}$ is the sequence of random rainfall depths with distribution given by (5), and $\{\tau_i = t_i - t_{i-1}, i = 1, 2, 3, \ldots\}$ is the interarrival time sequence of a stationary Poisson process with rate λ.

2.2. Interception

A considerable amount of rainfall is intercepted by the aerial part of vegetation, the remaining directly reaches the soil as throughfall. Especially in arid and semiarid climates, where rainfall events are generally short and evaporation demand is high, a sizeable fraction of the intercepted rainfall is lost directly through evaporation, while the rest reaches the soil as stem flow (e.g., [16,59,68]). The precise mechanisms of interception are quite complicated to model and depend on vegetation type as well as on the intensity and duration of rainfall. Because of its strong dependence on the type of plant and more specifically on its leaf area index, the amount lost by interception can indeed be quite different for, say, trees and grasses. As an example, well-vegetated trees in South-African savannas can intercept over to 0.2 cm of rainfall per storm event [60], while grasses usually intercept much less. At small spatial scales interception is also known to alter the spatial distribution of the water reaching the soil (e.g., through stem flow and crown shading; [59]), but we do not consider these effects in this paper.

In order to keep analytical tractability, interception will be incorporated in the stochastic model by simply assuming that, depending on the kind of vegetation, a given amount of water can be potentially intercepted from each rainfall event. This implies fixing a threshold for rainfall depth, Δ, below which no water reaches the ground. If the depth of a given rainfall event, h_i, is higher than Δ, then the actual rainfall depth reaching the soil is assumed to be $h_i - \Delta$, and Δ is lost by interception. The amount of water intercepted can be related to the type of vegetation simply by using different values for Δ. The model of interception is sketched in Fig. 2(a) using $\Delta_t = 0.2$ and $\Delta_g = 0.05$ cm, for trees and grasses, respectively. The effect of wind and air temperature on interception losses are negligible compared to the role of differences in canopy coverage. Although admittedly being a simplistic model for interception, the previous scheme provides a representation of the process which is in good agreement with the experimental evidence. As shown in Fig. 2(b), the percentage of rainfall intercepted as a function of total rainfall reproduces well the one found in field experiments (e.g., [19,31]).

From a mathematical viewpoint the consideration of a threshold on the rainfall Poisson process does not complicate its analytical tractability. The rainfall process is in fact transformed into a new marked-Poisson process, called a censored process, where the frequency of rainfall events is now

$$\lambda' = \lambda \int_\Delta^\infty f_H(h)\,\mathrm{d}h = \lambda\,\mathrm{e}^{-\Delta/\alpha} \tag{8}$$

and the depths h' have the same distribution as h, given by Eq. (5). Thus, one can simply write

$$R(t) - I(t) = \sum_i h_i'\delta(t - t_i'), \tag{9}$$

where $\{\tau_i' = t_i' - t_{i-1}', i = 1, 2, 3, \ldots\}$ is the interarrival time sequence of a stationary Poisson process with frequency λ'.

2.3. Infiltration and runoff

It is assumed that, when the soil has enough available storage to accommodate the totality of the incoming rainfall event, the increment in water storage is equal to the rainfall depth of the event; whenever the rainfall depth exceeds the available storage, the excess is converted in surface runoff. Since it depends on both rainfall and soil moisture content, infiltration from rainfall results to be a stochastic, state-dependent component, whose magnitude and temporal occurrence are controlled by the entire soil moisture dynamics. We do not consider the temporal propagation of the wetting front
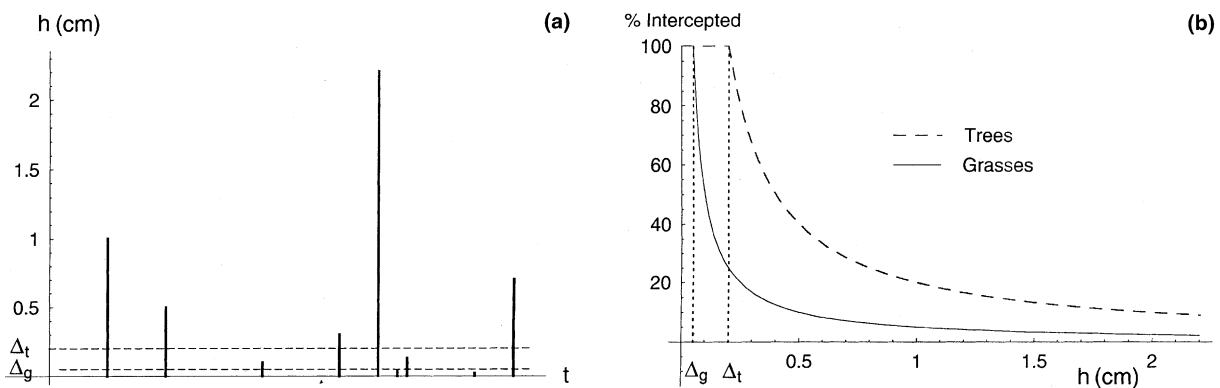

Fig. 2. Representation of the modeling scheme adopted for interception: (a) temporal sequence of rainfall events (h is the rainfall depth) along with the thresholds of interception, Δ_t and Δ_g, typical for trees and grasses; (b) typical example of the percentage of intercepted rainfall as a function of the total rainfall per event.

into the soil, because of the vertically lumped representation of soil moisture dynamics. However, this is not judged to be too restrictive when the soil moisture dynamics is considered at the daily time scale.

The probability distribution of the infiltration component may be easily written in terms of the exponential rainfall-depth distribution (5) and soil moisture state s. If we refer, for future convenience, to its dimensionless counterpart y (i.e., the infiltrated depth of water normalized by nZ_r) we can write

$$f_Y(y,s) = \gamma e^{-\gamma y} + \delta(y - 1 + s)$$
$$\times \int_{1-s}^{\infty} \gamma e^{-\gamma u} \, du \quad \text{for } 0 \leqslant y \leqslant (1-s), \qquad (10)$$

where γ is defined in Eq. (6). The mass at $(1-s)$ represents the probability that a storm will produce saturation when the soil has moisture s (Fig. 3). This sets the upper bound of the process at $s = 1$, making the soil moisture balance evolution – e.g., Eq. (1) – a bounded shot noise process. Although the bounded character of the process would at first seem to make it quite complex from a mathematical viewpoint, the Markovian nature of the process allows for a complete analytical solution, at least in the case of steady-state conditions, as will be discussed later on.

Similarly to Eq. (9), infiltration from rainfall can be written in Eq. (1) as

$$\varphi[s(t), t] = nZ_r \sum_i y_i \delta(t - t_i'), \qquad (11)$$

where $\{y_i, i = 1, 2, 3, \ldots\}$ is the sequence of random infiltrations having distribution (10).

The probabilistic analysis of the temporal distribution of runoff production resulting from the process implies the study of the crossing properties of the level $s = 1$, along the lines that will be discussed in the third part of this series [51]. We only notice here that the runoff process by itself is not Markovian, and the temporal distribution of its time of occurrence is not exponential.

It is worth noticing that runoff production may also be interpreted in a different but equivalent manner by considering an alternative process where runoff occurs from deterministic losses which take place at an infinite rate above $s = 1$. In this case the state variable s is not required to be formally bounded at $s = 1$, as the instantaneous decay above $s = 1$ makes the process completely equivalent to the bounded one for $s < 1$. This interpretation will turn out to be useful for a more intuitive interpretation of some of the results that will be obtained.

2.4. Active soil depth

The soil is modeled as an horizontal layer of depth Z_r with homogeneous characteristics. The product of soil depth and porosity defines the active soil depth, nZ_r, which is the height (or volume per unit surface area) available for water storage. From a physical viewpoint, the active soil depth in Eq. (1) represents the inertia of the system and, as such, controls the temporal scale of the system response. As will be seen in detail later, different values of nZ_r greatly affect the response and interaction of soil and vegetation to climate forcing. It is interesting to point out how the intermittent nature of the forcing, which makes the system undergo continuous fluctuations, leads to the aforementioned role of the active soil depth, even in statistically steady conditions. From a mathematical viewpoint, this important interplay between temporal forcing and soil depth can be understood from Eq. (1) by noticing that, if the infiltration from rainfall had been constant in time, instead of being intermittent, the steady condition would have been independent of soil depth.

The values of porosity and soil depth are generally influenced by many factors. Porosity usually shows some dependence on soil texture; plant roots and the action of small animals may also alter the value of the so-called macroporosity and produce preferential direction for water movement. However, since the effective importance of these latter variations of porosity are difficult to quantify without making the modeling scheme restrictively specific, we will refer only to variations due to different soil textures (see Table 1).

The actual soil depth involved in the water balance is a difficult parameter to estimate and may show a large range of spatial variation, depending on soil pedology and, especially, vertical root distribution (e.g., [7,28,63]). Thus, we will not fix a priori the values of Z_r, but rather consider a range of possible values estimated from field observations, according to the type of vegetation present at the site. As a general rule, trees generally have deeper roots than grasses, and tend to be accompanied by a slightly higher effective soil porosity (see Fig. 1).
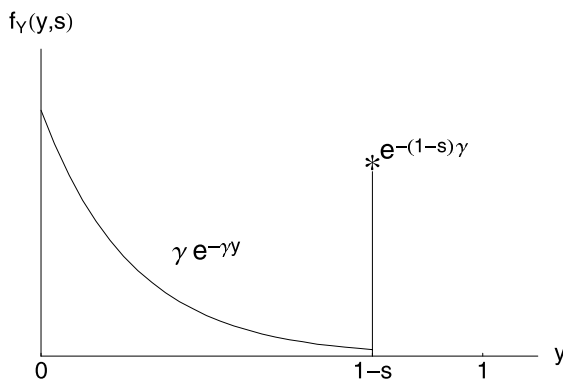

Fig. 3. Sketch of the probability density function describing infiltration from rainfall y. The asterisk represents the atom of probability corresponding to soil saturation.

Table 1
Parameters describing various soil characteristics used in the model for four different soil textures[a]

	$\overline{\Psi}_s$[b] (MPa)	$\overline{\Psi}_s$(log)[b], (MPa)	b[b]	c[b]	K_s[c] (cm/d)	n[d]	β	s_h	s_w	s^*	s_{fc}
Sand	-1.85×10^{-3}	-0.34×10^{-3}	4.05	11.1	>200	0.35	12.1	0.08	0.11	0.33	0.35
Loamy sand	-0.88×10^{-3}	-0.17×10^{-3}	4.38	11.7	$\approx$100	0.42	12.7	0.08	0.11	0.31	0.52
Sandy loam	-2.10×10^{-3}	-0.70×10^{-3}	4.90	12.8	$\approx$80	0.43	13.8	0.14	0.18	0.46	0.56
Loam	-4.68×10^{-3}	-1.43×10^{-3}	5.39	13.8	$\approx$20	0.45	14.8	0.19	0.24	0.57	0.65
Clay	-3.97×10^{-3}	-1.82×10^{-3}	11.4	25.8	<10	0.5	26.8	0.47	0.52	0.78	$\approx$1

[a] The values of s_h, s_w, and s^* have been calculated supposing a soil water potential $\Psi_{s,s_h} = -10$ MPa, $\Psi_{s,s_w} = -3$ MPa, and $\Psi_{s,s^*} = -0.03$ MPa, respectively; s_{fc} is the s level at which the leakage losses become negligible with respect to the evapotranspiration losses (see text for details).
[b] Data reference: Clapp and Hornberger [8].
[c] The values reported are those typical found in the literature, e.g., [15, pp. 80–81]; [26, p. 8]; [31].
[d] Data from: Dingman [16, p. 215]; Lai and Katul [31]; Cosby et al. [10].

A number of links and feedbacks between vegetation, climate, and soil will not be considered in this analysis, being of secondary importance at the time scale we are concerned with. For analyzes focusing on the long-term evolutionary dynamics of vegetation, however, one should take into account the variations of porosity, soil aging, and soil depth, which are linked to soil production and litter decomposition and in turn also to soil moisture dynamics. Such variations generally take place at much longer timescales than the ones considered here, but can become faster in tropical ecosystems (e.g., [34]). In those cases, nZ_r and the other soil characteristics should not be considered static parameters, but evolving variables.

The relevance of the active soil depth has also been emphasized in what concerns its role on large-scale soil moisture dynamics and its relevant ecological consequences. Milly and Dunne [40] and Milly [39] have studied the effect of soil depth on the global water balance and its response to climate change. Nepstad et al. [42], Canadell et al. [7], and Scholes and Archer [59] have dealt with the impact of soil depth on the vegetation stress and on the possible selection of temporal niches of soil–moisture availability by different vegetation types.

2.5. Evapotranspiration

Since interception has already been subtracted, the term $E(s,t)$ in Eq. (3) represents the sum of the losses resulting from plant transpiration and evaporation from the soil. Although these are governed by different mechanisms, we will not consider them separately, but rather we will model evapotranspiration as the sum of the two. At very low levels of soil moisture, when plants stop transpiring (i.e., below the so-called wilting point s_w), we will speak only of evaporation.

When soil moisture is high, the evapotranspiration rate depends mainly on the type of plant and climatic conditions (e.g., wind speed, air temperature and humidity, etc.). As long as soil moisture content is sufficient to permit the normal course of the plant physiological processes, evapotranspiration is assumed to occur at a maximum rate E_{max}, which is independent of s. When soil moisture content falls below a given point s^*, which, as we shall see, depends on both vegetation and soil characteristics, plants start reducing transpiration closing their stomata to prevent internal water losses (e.g., [25,34,44,61,66]). Below s^*, soil water availability becomes a key factor in determining the actual evapotranspiration. Photosynthesis-related transpiration and root water uptake continue at a reduced rate until soil moisture reaches the wilting point s_w. At this level, suction to extract water from soil is so high that it damages the plant tissues (e.g., [33,44,61]). Small water losses from the plant continue via cuticular transpiration and, if soil water is not replenished by rainfall, wilting and irreversible plant damages begin to appear. We will discuss in more detail the plant response to water stress in the third part of this series [51]. Below wilting point, s_w, soil water is further depleted by evaporation only at a very low rate up to the so-called hygroscopic point, s_h.

Even though the rate of transpiration below s^* is reduced through complex mechanisms and feedbacks, exerted at different levels by each particular plant (and involving also wind speed, air humidity, temperature, and radiation at the site), the relationship between the rate of plant water uptake and soil moisture content between s^* and s_w is well approximated by a linear decrease (e.g., [25,61]). Fig. 4 shows an example of the relationship between leaf conductance and soil moisture content measured during a controlled experiment. The strongly nonlinear, threshold-like dependence of the transpiration rate on soil moisture content is clearly evident. Since, under normal conditions, leaf conductance exerts the most important control on transpiration (e.g., [29,45]) – to the point that the transpiration rate is practically proportional to leaf conductance – the same kind of dependence on soil moisture is also to be expected for transpiration, when the water vapor deficit is kept constant. Notice also from Fig. 4 that the soil moisture level at incipient stomatal closure does not sensibly change notwithstanding the relevant variations
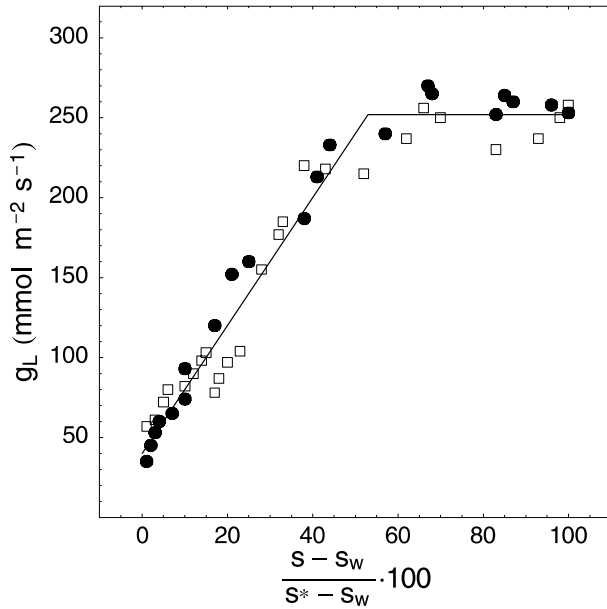
Fig. 4. Leaf conductance g_L vs soil moisture level for *Nerium oleander*, measured maintaining two different levels of vapor pressure deficit (solid circles and open squares, respectively). Adapted from [61], and after [23].

Fig. 5. Behavior of soil water losses (evapotranspiration and leakage), $\chi(s)$, as function of relative soil moisture for typical climate, soil and vegetation characteristics in semiarid ecosystems.

of the vapor pressure deficit. For most of the plants in temperate and semiarid regions, similar experimental evidences of this typical behavior can be found in the literature, both at the level of the single plant and of the entire stand (e.g., [20–22,50,62,67]). Due to different and specialized photosynthetic pathways (e.g., the CAM pathway), notable exceptions to this behavior have been reported in extremely arid regions (e.g., [34,36]), so that suitable modifications should be considered for the analogous modeling of transpiration vs soil moisture in particular species of desert flora.

From the above discussion, losses from evapotranspiration will be assumed to happen at a constant rate E_{max} for $s^* < s < 1$, and then to linearly decrease with s, from E_{max} to a value E_w at s_w. Below s_w, only evaporation from the soil is present and the loss rate is assumed to decrease linearly from E_w to zero at s_h. The dependence of evapotranspiration losses on soil moisture is summarized in the following expression

$$E(s) = \begin{cases} E_w \frac{s - s_h}{s_w - s_h}, & s_h < s \leqslant s_w, \\ E_w + (E_{max} - E_w)\frac{s - s_w}{s^* - s_w}, & s_w < s \leqslant s^*, \\ E_{max}, & s^* < s \leqslant 1, \end{cases} \quad (12)$$

whose behavior is shown in Fig. 5. The introduction of the two new thresholds s_w and s_h and the distinction between transpiration and evaporation at low soil moisture levels represent an important modification to the model presented in Rodriguez-Iturbe et al. [54]. This improvement is necessary to represent better the soil moisture dynamics under drought conditions as well as for the related analysis of the crossing properties of the
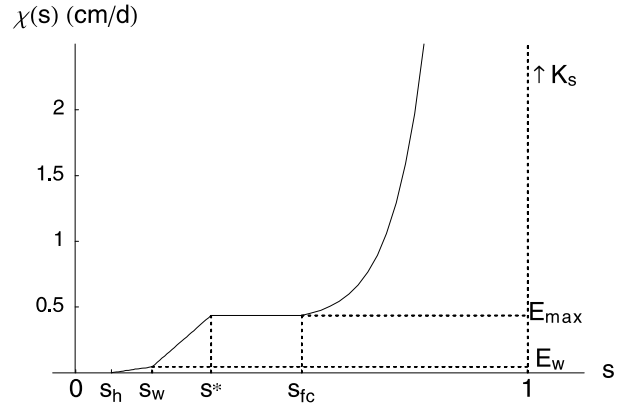
wilting point level. In the previous version of the model the evapotranspiration losses decrease linearly from E_{max} at s^* to zero at zero soil moisture, and thus the losses at low levels of soil water contents are somewhat overestimated. With the present improvements the amount of water unavailable to plants below wilting point is realistically taken into consideration. As will be seen in the following discussion concerning the role of soil texture, this amount can be considerable when the soil contains large percentages of clay.

The smallest timescale of interest under the framework of the present model is the daily scale. Thus no consideration is made of hourly fluctuations in evapotranspiration rates and hence we refer to daily average values of E_{max}. These values will be assumed to be approximately constant during the growing season. As for the case of the rainfall input, when dealing with growing seasons of four or more months it may be necessary to use different parameters for evaporation losses in the early and the later part of the growing season. Possible estimates of E_{max} values may be obtained using physically-based expressions, such as the Penman–Monteith equation, relating atmospheric demand and leaf conductance (e.g., [4,16,20,21]). However, because of the uncertainty in applying these theoretical expressions [4], in the following we prefer to refer to measured data, analogously to what is done, for example, by Paruelo and Sala [50]. For regions with hot growing seasons, values of E_{max} are typically around 0.5 cm/d for grasses and 10% less for trees (e.g., data from [60]). Of this total value approximately 0.1 cm/d can be attributed to evaporation from the soil (e.g., [45, p. 360]). Particular values of evapotranspiration rates for different water-controlled ecosystems will be discussed in the applications presented in Part IV of this series [32]. The higher maximum transpiration rate of grasses in these regions is partly explained by the more efficient C_4 pathway of photosynthesis that many grasses of semiarid ecosys-

tems have with respect to the more common and less efficient C_3 pathway of trees. It is good to remark that the values of E_{max} refer to evapotranspiration rates representative of a unitary surface uniformly covered with vegetation.

Both the value of soil moisture s^* at which transpiration starts being reduced and the wilting point s_w depend on the type of vegetation as well as on the soil properties. An indication of their possible values can be obtained from the soil–plant–atmosphere continuum scheme, which describes the transfer of water by plants from soil to atmosphere in terms of the water potential, Ψ (e.g., [34,45,47,65]). Any given plant is characterized by typical levels of plant water potential below which evapotranspiration is reduced and finally stopped. Neglecting hourly diurnal fluctuations (e.g., [34, p. 247]), and using only average daily values, plant water potential can be related to soil matric potential, Ψ_s (see Part III of this series). Thus, for each type of plant, one can fix typical values of soil matric potential, Ψ_{s,s^*} and Ψ_{s,s_w}, at which stomatal closure begins and is completed, respectively. Soil matric potential can then be related to relative soil moisture using the soil–water retention curves (e.g., [8,16,27]). Such curves depend on the type of soil, and this provides the dependence of s^* and s_w on soil texture.

In general, wilting point for plants in water-controlled ecosystems under natural conditions are considerably lower than the value of -1.5 MPa commonly assumed for temperate crops. For plants in semiarid environments, typical values of soil matric potential at the wilting point, Ψ_{s,s_w}, can reach values as low as -3 MPa or even -5 MPa (e.g., [34–36,53,60]). There is considerable variation among different plants, but the permanent wilting point is generally lower for grasses than for trees, even though grasses undergo water stress conditions before trees do. There are fewer available data for Ψ_{s,s^*}, which in some water-restricted ecosystems is estimated to be around -0.03 MPa, with values somewhat larger for grasses than for trees (e.g., [60]).

As explained above, the values of s^* and s_w can be deduced from the soil–water retention curves. Following Clapp and Hornberger [8] one can use empirically-determined soil–water retention curves of the form

$$\Psi_s = \bar{\Psi}_s s^{-b} \tag{13}$$

where $\bar{\Psi}_s$ and b are experimentally determined parameters (see Table 1). Typical curves for loamy sand and loam are shown in Fig. 6. It is worth noticing that, in order to obtain values of s_w and s^* in reasonable agreement with measured field data, one should use $\bar{\Psi}_s$ as given by the geometric mean of the measured values (reported by Clapp and Hornberger [8, p. 603]) instead of its arithmetic mean, which would yield unrealistically high values of soil moisture. As can be seen from Fig. 6,
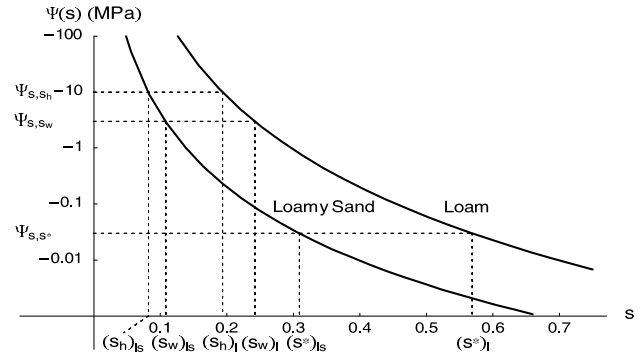

Fig. 6. Soil–moisture retention curves used to derive values of the soil water levels s_h, s_w, and s^* from the correspondent values of soil matrix potential, $\Psi_{s,s_h} = -10$ MPa, $\Psi_{s,s_w} = -3$ MPa, $\Psi_{s,s^*} = -0.03$ MPa. Two different soil types, a loamy sand and a loam, are considered, using the parameters reported in Table 1.

the role of soil texture is very important. Different types of soil may yield very different levels of relative soil moisture corresponding to the same value of soil matric potential. Typical values of s_w are found around 0.1 for loamy sand, while for loam they are near 0.25. Similarly, s^* is found around 0.3 for loamy sand and moves above 0.55 in the case of loam (see Table 1). The values of s_w and s^* are crucially important both in the water balance and in the study of plant water stress. The previous example clearly shows how the transpiration control by vegetation, besides depending on physiological plant characteristics, directly passes through soil properties.

Let us finally discuss possible values of E_w and s_h. In this regard it is important to notice that the small losses involved in this phase of the dynamics [48,49] make their precise values not very important for the temporal evolution of the soil moisture process and the different components of the water balance, as long as a correct order of magnitude is used in their description. Thus, we will not go in a detailed analysis toward a precise estimation and simply use a value of -10 MPa for Ψ_{s,s_h} and 0.01 cm/d for E_w. The value of s_h can be obtained from Ψ_{s,s_h} using the soil–water retention curves in the same way as for s_w and s^* (see Fig. 6).

A final comment is in order concerning the temporal interplay of rainfall and evapotranspiration and, in particular, the fact that evapotranspiration is considerably reduced throughout the duration of precipitation events. This aspect, which would be a source of further complication if one considered the specific temporal dynamics within the rainfall event, is not relevant in the present model since rainfall is modeled as a sequence of instantaneous pulses, while evapotranspiration takes place continuously. Thus in our mathematical framework the instantaneous contribution of evapotranspiration is infinitesimal compared to that of rainfall in Eq. (1) whenever there is a precipitation event. This might lead to a slight overestimation of the total evapotranspiration.

2.6. Leakage losses

Leakage losses are assumed to happen by gravity at the lowest boundary of the soil layer, neglecting possible differences in matric potential between the soil layer under consideration and the one immediately below. The loss rate is assumed to be at its maximum when soil is saturated and then rapidly decay as the soil dries out, following the decrease of the hydraulic conductivity $K(s)$. The decay of the hydraulic conductivity is normally modeled using empirical relationship of different forms (e.g., [64,27]). We will assume here that the hydraulic conductivity decays exponentially from a value equal to the saturated hydraulic conductivity K_s at $s = 1$, to a value of zero at a field capacity, s_{fc}. The exponential form, here chosen for reasons of mathematical tractability, has been commonly employed in the literature (e.g., [11,14,64]) as an alternative to the more customary power law. The assumed behavior of leakage losses is thus expressed as

$$K(s) = L(s) = \frac{K_s}{e^{\beta(1-s_{fc})} - 1}\left[e^{\beta(s-s_{fc})} - 1\right],$$
$$s_{fc} < s \leqslant 1, \tag{14}$$

where β is a coefficient which is used to fit the above expression to the power law (e.g., [8,16,27])

$$K(s) = K_s s^c \tag{15}$$

with $c = 2b + 3$ and b defined in Eq. (13). A possible criterion to minimize the discrepancies between the two expressions (14) and (15) is to impose the condition that they subtend the same area between s_{fc} and $s = 1$. This provides $\beta = 2b + 4$ so that the value of β depends on the type of soil, varying from 12 for sand to 26 for clay. Using the typical values reported in Table 1, the two expressions have very similar behavior.

The field capacity s_{fc} (for a discussion of its physical and practical relevance see [27]) is operationally defined as the value of soil moisture at which the hydraulic conductivity becomes negligible (here 10%) compared to the maximum daily evapotranspiration losses E_{max} (for this purpose assumed to be 0.5 cm/d). The power-law relationship (15) has been used to estimate s_{fc} in the manner described above.

The behavior of leakage losses is represented in Fig. 5. The strong nonlinear behavior of these losses as a function of soil moisture content is evident. This representation is a considerable improvement with respect to the linear decay of the leakage losses used in the model by Rodriguez-Iturbe et al. [54]. This new description allows for a representation of the soil moisture dynamics at high levels of soil moisture more realistically linked to the soil characteristics.

From a physical viewpoint, the modeling of leakage driven by a unit vertical gradient due to gravity implies no interaction with the underlying soil layers and the water table. Such simplification may pose some restrictions in the applications of the model, even though in most water-controlled ecosystems the contribution due to capillary rise from the water table or deeper soil layers is generally of secondary importance. The actual applicability of the modeling scheme needs to be assessed case by case.

2.7. Soil-drying process

During inter-storm periods the model (1) describes deterministic decays of soil moisture starting from initial values which depend on the depth of last rainfall event and on the previous history of the entire process. Upon normalization with respect to the active soil depth, the complete form of the losses described in the previous paragraphs is summarized as follows

$$\rho(s) = \frac{\chi(s)}{nZ_r} = \frac{E(s) + L(s)}{nZ_r}$$

$$= \begin{cases} 0, & 0 < s \leqslant s_h, \\ \eta_w \frac{s-s_h}{s_w-s_h}, & s_h < s \leqslant s_w, \\ \eta_w + (\eta - \eta_w)\frac{s-s_w}{s^*-s_w}, & s_w < s \leqslant s^*, \\ \eta, & s^* < s \leqslant s_{fc}, \\ \eta + m(e^{\beta(s-s_{fc})} - 1), & s_{fc} < s \leqslant 1, \end{cases} \tag{16}$$

where $\rho(s)$ stands for the dimensionless loss function to which we will refer hereafter, and

$$\eta_w = \frac{E_w}{nZ_r}, \tag{17}$$

$$\eta = \frac{E_{max}}{nZ_r}, \tag{18}$$

$$m = \frac{K_s}{nZ_r(e^{\beta(1-s_{fc})} - 1)}. \tag{19}$$

Before studying the probabilistic structure of the overall process, it is useful to analyze the behavior of the system in absence of rainfall. We focus now on the physically interesting condition of a prolonged drought following a rainy period. The analytical expression for the soil moisture decay from an initial condition $s_0 \geqslant s_{fc}$ in absence of rainfall events is

$$s(t) = \begin{cases} s_0 - \frac{1}{\beta}\ln\left[\frac{(\eta-m+me^{\beta(s_0-s_{fc})})e^{\beta(\eta-m)t} - me^{\beta(s_0-s_{fc})}}{\eta-m}\right], \\ \quad 0 \leqslant t < t_{s_{fc}}, \\ s_{fc} - \eta(t - t_{s_{fc}}), \\ \quad t_{s_{fc}} \leqslant t < t_{s^*}, \\ s_w + (s^* - s_w)\left[\frac{\eta}{\eta-\eta_w}\exp\left(-\frac{\eta-\eta_w}{s^*-s_w}(t-t_{s^*})\right) - \frac{\eta_w}{\eta-\eta_w}\right], \\ \quad t_{s^*} \leqslant t < t_{s_w}, \\ s_h + (s_w - s_h)\exp\left(-\frac{\eta_w}{s_w-s_h}(t-t_{s_w})\right), \\ \quad t_{s_w} \leqslant t < \infty, \end{cases} \tag{20}$$

where

$$t_{s_{\mathrm{fc}}} = \frac{1}{\beta(m-\eta)}\left[\beta(s_{\mathrm{fc}}-s_0) + \ln\left(\frac{\eta - m + m\,\mathrm{e}^{\beta(s_0-s_{\mathrm{fc}})}}{\eta}\right)\right],$$

$$t_{s^*} = \frac{s_{\mathrm{fc}} - s^*}{\eta} + t_{s_{\mathrm{fc}}}, \tag{21}$$

$$t_{s_{\mathrm{w}}} = \frac{s^* - s_{\mathrm{w}}}{\eta - \eta_{\mathrm{w}}}\ln\left(\frac{\eta}{\eta_{\mathrm{w}}}\right) + t_{s^*}$$

represent the time to evolve, in absence of rainfall, from s_0 to s_{fc}, s^*, and s_{w}, respectively. Notice that, since the moisture decays exponentially to s_{h}, the process will only be at $s = s_{\mathrm{h}}$ if it starts at that value. Fig. 7(a) and (b) show examples of Eq. (20) starting from saturated conditions. One can clearly see the remarkable control exerted both by the soil texture and the active depth nZ_{r}. Under the same climatic conditions and with the same vegetation type (i.e., same $E_{\max}$, $\Psi_{\mathrm{s},s_{\mathrm{w}}}$, and Ψ_{s,s^*}) the time to reach the wilting point in the absence of precipitation can vary from around 20 days for a shallow loamy sand, up to well beyond 60 days for a deep loamy soil. It is also interesting to notice the different role of soil texture on the water availability for vegetation. On one hand, because of its lower hydraulic conductivity, a finer soil increases soil water availability and thus the time to reach the wilting point; on the other hand, the higher values of s_{h}, s_{w}, and s^* lead to an increase in the amount of residual water which is not extractable for plant transpiration.

3. Equilibrium distributions of soil moisture

The stochastic rainfall forcing in Eq. (1) makes its solution meaningful only in probabilistic terms. The probability density function of soil-moisture $p(s,t)$ can be derived from the Chapman–Kolmogorov forward equation for the process under analysis. We will not go into the details of this derivation and refer to the paper by Rodriguez-Iturbe et al. [54] for a detailed description of its construction.

The Chapman–Kolmogorov forward equation for the evolution of probability of $s \geqslant s_{\mathrm{h}}$ is [54]

$$\frac{\partial}{\partial t}p(s,t) = \frac{\partial}{\partial s}[p(s,t)\rho(s)] - \lambda'p(s,t) + \lambda'\int_{s_{\mathrm{h}}}^{s} p(u,t)f_Y(s-u;u)\,\mathrm{d}u, \tag{22}$$

where we have put equal to zero the atom of probability at $s = s_{\mathrm{h}}$, assuming that the process never starts at $s = s_{\mathrm{h}}$. The various terms on the r.h.s of the above integro-differential equation represent the contributions to $p(s,t)\,\mathrm{d}s$ of the different mechanisms of the soil moisture process. The first term is related to the gain of probability due to the drift of the pdf in the deterministic decay $\rho(s)$, the second term represents the loss of probability due to possible jumps with frequency λ' which cause the process to leave the given trajectory at the level s at time t, and the last term is the positive contribution to the probability due to jumps to level s starting from lower soil moisture values.

The complete solution of Eq. (22) presents serious mathematical difficulties and only formal solutions in terms of Laplace transforms have been obtained for simple cases when the process is not bounded at $s = 1$ ([12] and references therein). Thus we will not consider here transient conditions for the soil moisture process, but rather concentrate on the steady-state case. On taking the limit as $t - \infty$ Eq. (22) one obtains

$$\frac{\mathrm{d}}{\mathrm{d}s}[\rho(s)p(s)] - \lambda'p(s) + \lambda'\int_{s_{\mathrm{h}}}^{s} p(u)f_Y(s-u,u)\,\mathrm{d}u = 0, \tag{23}$$

which, using Eq. (10) yields

$$\frac{\mathrm{d}}{\mathrm{d}s}[\rho(s)p(s)] - \lambda'p(s) + \lambda'\int_{s_{\mathrm{h}}}^{s} p(u)\gamma\,\mathrm{e}^{-\gamma(s-u)}\,\mathrm{d}u$$
$$+ \delta(s-1)\lambda'\int_{s_{\mathrm{h}}}^{s} p(u)\gamma\,\mathrm{e}^{-\gamma(1-u)}\,\mathrm{d}u = 0. \tag{24}$$
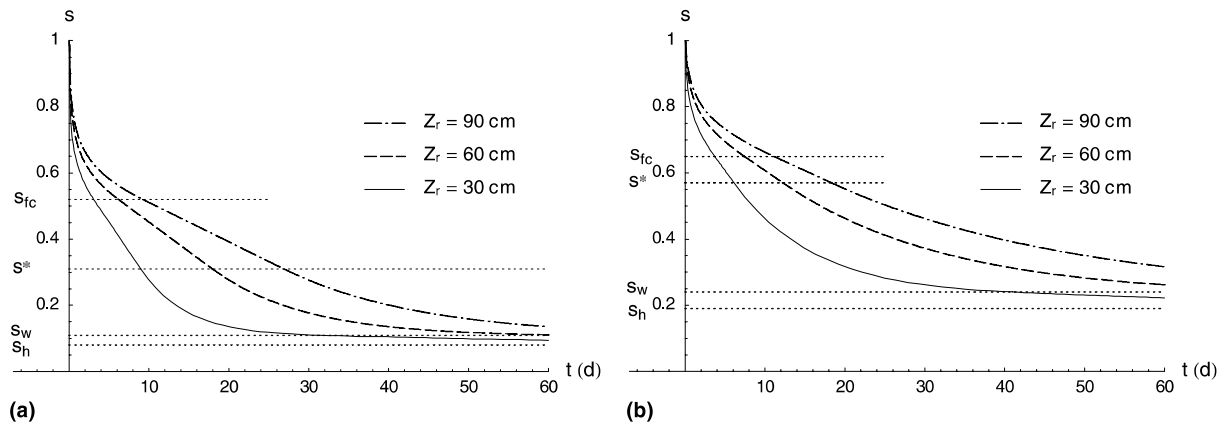

Fig. 7. Plots of the solutions of the soil-drying process for a loam (a) and loamy sand (b) having different values of active soil depth (30, 60, and 90 cm). The parameters used are $E_{\max} = 0.45$ cm/d, $E_{\mathrm{w}} = 0.01$ cm/d. The values of s_{h}, s_{w}, s^*, s_{fc}, n, β, and K_s are reported in Table 1.

For $s < 1$, Eq. (24) is equivalent to the ordinary differential equation [54]

$$\frac{d}{ds}[\rho(s)p(s)] + \gamma\rho(s)p(s) - \lambda'p(s) = 0, \tag{25}$$

that, compared with Eq. (24), yields

$$\gamma\rho(s)p(s) = \lambda' \int_{s_h}^{s} p(u)\gamma e^{-\gamma(s-u)}\,du. \tag{26}$$

For $s = 1$, Eq. (24) becomes

$$p(1)\frac{d}{ds}\rho(s)|_{s=1} + p(1)p(1)\delta(0) - \lambda'p(1) + \lambda'$$
$$\times \int_{s_h}^{1} p(u)\gamma e^{-\gamma(1-u)}\,du + \delta(0)\lambda'$$
$$\times \int_{s_h}^{1} p(u)\gamma e^{-\gamma(1-u)}\,du = 0. \tag{27}$$

Dividing by $\delta(0)$ and neglecting the infinitesimal terms one obtains

$$\gamma\rho(1)p(1) = \lambda' \int_{s_h}^{1} p(u)\gamma e^{-\gamma(1-u)}\,du, \tag{28}$$

which turns out to be the same as Eq. (26) calculated in $s = 1$. Eqs. (25) and (26) are both valid for the bounded and unbounded case, whose solutions therefore only differ for an arbitrary constant of integration. In fact, the general form of the solution is

$$p(s) = \frac{C}{\rho(s)} e^{-\gamma s + \lambda' \int \frac{du}{\rho(u)}} \quad \text{for } s \geqslant s_h, \tag{29}$$

where C is the constant of integration. The value of such constant can be simply obtained by imposing the normalizing condition

$$\int_{s_h}^{1} p(s)\,ds = 1. \tag{30}$$

Notice that all the complication brought by the presence of the bound at $s = 1$ is contained in the integration constant and the only effect of the saturation of the soil at $s = 1$ is the restricted range over which $p(s)$ is normalized in (30). The explanation for this lies in the Markovian nature of the soil moisture process. If excursions of the process above 1 are impossible, the process will spend more time in states $s \leqslant 1$ than would be the case otherwise, but the relative proportions of times in those states will be unchanged. Imagine two processes with, and without, the restriction that s is bounded to values less than one. In the latter case, trajectories of the soil moisture process will jump above the level $s = 1$ and, eventually, drift down across this level once more. In the former case, these excursions are effectively excised, as the process jumps only to $s = 1$ and then immediately begins its downward decay. The trajectories below $s = 1$ in the two processes are indistinguishable.

The limits of the integral in the exponential term of Eq. (29) are chosen so to assure the continuity of $p(s)$ at the end points of the four different components of the loss function described by Eq. (16). Thus $p(s)$ obtained from Eq. (29) needs to be the same at the common end points of Eq. (16) although they are approached through different expressions of $\rho(s)$. In this manner the general solution is obtained as

$$p(s) = \begin{cases} \frac{C}{\eta_w}\left(\frac{s-s_h}{s_w-s_h}\right)^{\frac{\lambda'(s_w-s_h)}{\eta_w}-1}e^{-\gamma s}, \\ \qquad s_h < s \leqslant s_w, \\[1em] \frac{C}{\eta_w}\left[1 + \left(\frac{\eta}{\eta_w}-1\right)\left(\frac{s-s_w}{s^*-s_w}\right)\right]^{\frac{\lambda'(s^*-s_w)}{\eta-\eta_w}-1}e^{-\gamma s}, \\ \qquad s_w < s \leqslant s^*, \\[1em] \frac{C}{\eta}e^{-\gamma s + \frac{\lambda'}{\eta}(s-s^*)}\left(\frac{\eta}{\eta_w}\right)^{\frac{\lambda'\,s^*-s_w}{\eta-\eta_w}}, \\ \qquad s^* < s \leqslant s_{fc}, \\[1em] \frac{C}{\eta}e^{-(\beta+\gamma)s + \beta s_{fc}}\left(\frac{\eta e^{\beta s}}{(\eta-m)e^{\beta s_{fc}}+me^{\beta s}}\right)^{\frac{\lambda'}{\beta(\eta-m)}+1} \\ \qquad \times\left(\frac{\eta}{\eta_w}\right)^{\frac{\lambda'\,s^*-s_w}{\eta-\eta_w}}e^{\frac{\lambda'}{\eta}(s_{fc}-s^*)}, \\ \qquad s_{fc} < s \leqslant 1. \end{cases} \tag{31}$$

The expression of the constant C can be obtained analytically (see Appendix A). However, it is quite involved, due both to the piecewise form of the losses and to the presence of the bound. Likewise, we do not report here the expression for the mean of soil moisture. The behavior of the mean and variance were discussed at length by Rodriguez-Iturbe et al. [54] for the simpler model proposed in that paper. Although the present model has a more realistic description of leakage and evapotranspiration, the qualitative behavior is not changed.

The real utility of an analysis limited to steady-state conditions is related to the particular case considered. We do not discuss here cases where the transient dynamics may play a dominant role. It is important, however, to stress the conditions that need to be fulfilled for the application of the steady-state results. The first limitation is linked to the fact that climate is characterized by time invariant parameters throughout the growing season. The second consideration is related to the value of s at the start of the growing season. If this value is normally very different from the mean steady state condition, the relevance of the steady state solution will depend on the time it will take, on average, to go from the initial condition to values typical of the steady state. As will be seen below, this is related to the climatic conditions (e.g., seasonality), to the soil depth, and to the ratio between losses and rainfall input during the months preceeding the growing season.

The steady-state analysis is most appropriate for the study of water-controlled ecosystems where rainfall is mostly concentrated in a warm growing season, and winter is usually temperate and dry. As a consequence, the starting soil moisture condition at the beginning of

the growing season is not very different from the rest of the season and transients due to seasonality are generally not significant. In such cases most of the soil moisture dynamics takes place during the growing season, when plants have to compete among themselves and need to manage water losses (e.g., evaporation and leakage) to exploit the water infiltrating from rainfall. Different ecosystems which are examples of these conditions are the savannas of South Africa [60], the shrublands in Southern Texas, at least for a main portion of the growing season [2,59], and the shortgrass steppe in Colorado [56]. Nevertheless, transient soil moisture dynamics and climatic seasonality can be important in other semi-arid environments, especially at the beginning of the growing season. Typical cases include Mediterranean climates (e.g., [37,41,43]) and the Patagonian steppe [24,50]. Temperate forests in North-West United States (e.g., [68]) are also heavily controlled by transient soil moisture conditions. In these cases, rainfall and temperature are markedly out of phase, and

the dormant season thus becomes a period of consistent soil–water storage to be used during the following growing season.

Fig. 8 shows some examples of the pdf's derived from Eq. (31). The two different types of soil, already used for Figs. 6 and 7, are loamy sand and loam with two different values of active soil depth. These are chosen in order to emphasize the role of soil in the soil moisture dynamics. The parameters related to vegetation are kept fixed: a detailed discussion of the role of different functional vegetation types is postponed to the third and fourth parts of this series of papers. The role of climate is studied only in relation to changes in the frequency of storm events λ, while the mean rainfall depth α and the climatic control on E_{max} are kept constant. A coarser soil texture corresponds to a consistent shift of the pdf toward drier conditions, which in the most extreme case can reach a difference of 0.2 in the value of the mode. The shape of the pdf also undergoes marked changes. The broadest pdfs are found for shallower soils.
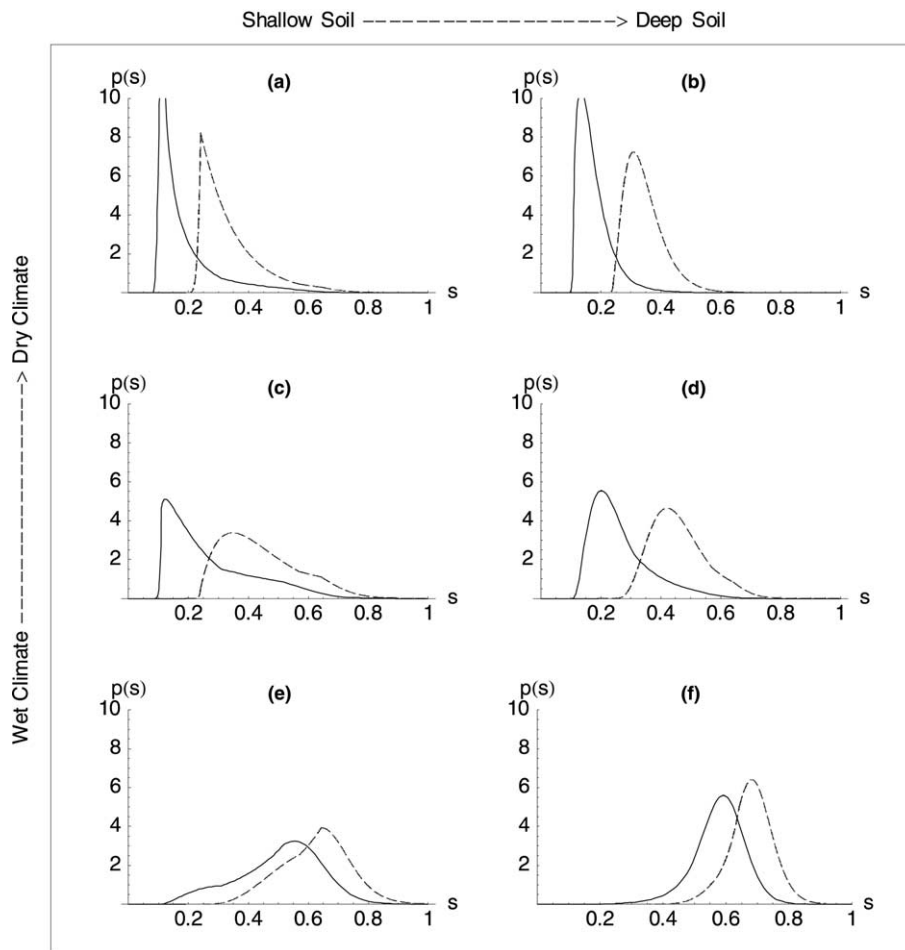

Fig. 8. Examples of pdfs of soil moisture for different type of soil, soil depth and mean rainfall rate. Continuous lines refer to loamy sand, dashed lines to loam (see Table 1 for the values of soil parameters). Left panels correspond to $Z_r = 30$ cm, right panel to 90 cm. Top, center, and bottom graphs have a mean rainfall rate λ of 0.1, 0.2 and 0.5 d^{-1}, respectively. Common parameters to all graphs are $\alpha = 1.5$ cm, $\Delta = 0$ cm, $E_w = 0.01$ cm/d, and $E_{max} = 0.45$ cm/d.

Although the qualitative behavior of the pdfs shown in Rodriguez-Iturbe et al. [54] is maintained, some important differences with the present, more realistic, model can be noticed as well. The main improvements are related to the tails of the distribution. At low levels of soil moisture the residual water content is directly related to the type of soil and vegetation present (see Fig. 8(a) in particular). At high soil moisture levels the more realistic representation of leakage provides smoother pdf's for wet conditions, and also yields slightly lower values of soil moisture as a result of an increased relevance of leakage.

We now focus on the possible impacts on vegetation of the probabilistic soil moisture dynamics represented on the pdfs of Fig. 8. A first indication of the importance of this aspect can be gained by studying the temporal evolution of soil moisture through the particular realizations corresponding to some of the pdfs just described. As an example, Fig. 9 shows a superposition of two traces of soil moisture with the same rainfall realization for the case of a loam with two different depths of active soil (the parameter values are those used for the broken line pdfs in Fig. 8(c) and (d)). In both cases the levels of soil moisture s^* and s_w are the same. The mean soil moisture is also approximately the same in both cases. The continuous line, corresponding to the deeper soil, is almost always between s^* and s_w, differently from the shallower soil where the trace lively jumps and decays between low and high soil moisture levels. Without anticipating a discussion on vegetation response, it is nevertheless impossible not to perceive the importance of such different soil moisture dynamics for different types of plants, and the possible implications for the development of different strategies of adaptation to water stress. A discussion of the impact of climate, soil,
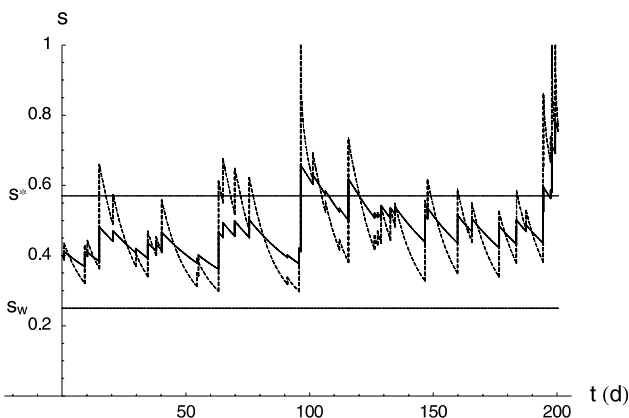

Fig. 9. Example of traces of soil moisture for the same rainfall sequence in a loamy soil with different depths ($\alpha = 1.5$ cm, $\lambda = 0.15$ d^{-1}, $\Delta = 0$ cm, $E_w = 0.01$ cm/d, $E_{max} = 0.45$ cm/d; see Table 1 for soil parameters). Continuous line refers to $Z_r = 90$ cm, dashed line to $Z_r = 30$ cm. The traces correspond to the pdfs reported with dashed line in Fig. 7(c) and (d).

and plant water uptake on vegetation response requires a more detailed analysis of the mechanisms of water stress and the definition of quantitative relationships to link such stress to soil moisture dynamics. This will be presented in Part III of this series [51].

4. Water balance

It is interesting to discuss the soil water balance resulting from the model presented here. In fact, the soil water balance is at the heart of many hydrologic problems and is of paramount importance in a wide range of issues, such as climate change and desertification, management of water resources, etc.

The different parts of the water balance are the long-term averages of the respective components of the soil moisture dynamics. As described in Eqs. (1)–(3), rainfall is first partitioned in interception, runoff, and infiltration into the soil. Infiltration is then divided into leakage and evapotranspiration. For purposes of describing vegetation conditions, the amount of water transpired can be further divided into water transpired under stressed conditions and water transpired under non-stressed conditions. This last distinction will be important Part III of this series of papers, in relation to the links between soil moisture dynamics and productivity of ecosystems. The long term average of Eq. (1) is simply

$$\langle \varphi \rangle - \langle \chi \rangle = 0. \tag{32}$$

Using Eqs. (2) and (3), the mean infiltration rate is

$$\langle \varphi \rangle = \langle R \rangle - \langle I \rangle - \langle Q \rangle, \tag{33}$$

where $\langle R \rangle, \langle I \rangle$, and $\langle Q \rangle$ stand for the mean rates of rainfall, interception, and runoff, respectively, while the average losses are

$$\langle \chi \rangle = nZ_r \int_{s_h}^{1} \rho(s)p(s)\,\mathrm{d}s. \tag{34}$$

The mean rainfall intensity is

$$\langle R \rangle = \alpha \cdot \lambda, \tag{35}$$

and the mean rate of interception is (see Section 2.2)

$$\langle I \rangle = \alpha \cdot (\lambda - \lambda') = \alpha\lambda\left(1 - \mathrm{e}^{-\Delta/\alpha}\right). \tag{36}$$

The water balance (32) can therefore be written as

$$\alpha \cdot \lambda' - \langle Q \rangle = \langle \chi \rangle \tag{37}$$

Returning to the mean rate of water losses from the soil $\langle \chi \rangle$, this can be also written as

$$\langle \chi \rangle = \langle E_s \rangle + \langle E_{ns} \rangle + \langle L \rangle$$
$$= nZ_r \int_{s_h}^{s^*} E(s)p(s)\,\mathrm{d}s + nZ_r \int_{s^*}^{1} E(s)p(s)\,\mathrm{d}s$$
$$+ nZ_r \int_{s_{fc}}^{1} L(s)p(s)\,\mathrm{d}s. \tag{38}$$

where $\langle E_s \rangle$, $\langle E_{ns} \rangle$, and $\langle L \rangle$ are the mean rate of evapo-transpiration under stressed conditions, the mean rate of non-stressed evapotranspiration and the mean rate of leakage, respectively.

Analytical expressions for the terms of Eq. (38) can be obtained using Eq. (25). Integrating equation (25) from s' to s'' one obtains

$$\int_{s'}^{s''} \rho(s)p(s)\,\mathrm{d}s = \frac{\lambda'}{\gamma}[P(s'') - P(s')] - \frac{1}{\gamma}[\rho(s'')p(s'') - \rho(s')p(s')], \tag{39}$$

where $P(s)$ is the cumulative density function of soil moisture, whose analytical expression is given in Appendix A. From Eq. (39) with $s' = s_h$ and $s'' = s^*$, the analytical expression of $\langle E_s \rangle$ can be calculated as

$$\langle E_s \rangle = nZ_r \int_{s_h}^{s^*} E(s)p(s)\,\mathrm{d}s = nZ_r \int_{s_h}^{s^*} \rho(s)p(s)\,\mathrm{d}s$$
$$= \alpha\lambda'P(s^*) - \alpha\eta p(s^*), \tag{40}$$

where the condition $\eta = \rho(s^*)$ (see (Eq. 16)) has been used. The evapotranspiration under non-stressed conditions can be obtained as

$$\langle E_{ns} \rangle = nZ_r \int_{s^*}^{1} E(s)p(s)\,\mathrm{d}s = nZ_r \eta \int_{s^*}^{1} p(s)\,\mathrm{d}s$$
$$= E_{\max}[1 - P(s^*)], \tag{41}$$

and the average leakage losses are

$$\langle L \rangle = nZ_r \int_{s_{fc}}^{1} L(s)p(s)\,\mathrm{d}s$$
$$= nZ_r \int_{s_{fc}}^{1} (\rho(s) - \eta)p(s)\,\mathrm{d}s$$
$$= \alpha\left[\lambda' - \lambda'P(s_{fc}) - \left(\eta + \frac{K_s}{nZ_r}\right)p(1) + \eta p(s_{fc})\right]$$
$$- E_{\max}[1 - P(s_{fc})], \tag{42}$$

where Eq. (39) has been used with $s' = s_{fc}$ and $s'' = 1$ (again from (16),

$$\rho(1) = \eta + \frac{K_s}{nZ_r} \quad \text{and} \quad \rho(s_{fc}) = \eta).$$

The total mean losses from the soil can now be calculated either by applying Eq. (39) with $s' = s_h$ and $s'' = 1$ (see Eq. (34)), or by summing Eqs. (40), (41), and (38) and simplifying the terms by the way of Eq. (35) with $s' = s_h$ and $s'' = s_{fc}$,

$$\langle \chi \rangle = \alpha\lambda' - \alpha\left(\eta + \frac{K_s}{nZ_r}\right)p(1). \tag{43}$$

Finally, Eqs. (37) and (43) allow one to write the mean runoff as

$$\langle Q \rangle = \alpha\left(\eta + \frac{K_s}{nZ_r}\right)p(1). \tag{44}$$

Fig. 10 presents examples of the behavior of the various components of the water balance normalized by the mean rainfall rate, for some specific rainfall, soil, and vegetation characteristics. The influence of the rainfall rate λ is shown in Fig. 10(a) for the case of a shallow loam. Since the amount of interception changes proportionally to the rainfall rate, it is not surprising that the fraction of water intercepted remains constant when normalized with the total rainfall, $\alpha \cdot \lambda$. The percentage of runoff increases almost linearly. More interesting is the interplay between leakage and the two components of evapotranspiration. The fraction of water transpired under stressed conditions rapidly decreases from $\lambda = 0.1$ to about $\lambda = 0.4$, while the evapotranspiration under non-stressed conditions evolves in a much more gentle manner. This last aspect has interesting implication for vegetation productivity. We will return to this problem in Part III of this series of papers. It appears clear that in semiarid conditions most of the water that actually reaches the soil is lost by evapotranspiration (in particular transpiration, see Section 2.5), a result in agreement with many field observations (e.g., [18,56,58,60]).

Fig. 10(b) shows the role of the active soil depth in the water balance. For relatively shallow soils we can notice a strongly nonlinear dependence on soil depth of all the components of the water balance (apart, of course, from interception, which is constant because the rainfall is constant). For example, passing from $nZ_r = 5$ to $nZ_r = 20$ the amount of water transpired is practically doubled.

Fig. 10(c) shows the impact on water balance when the frequency and amount of rainfall are varied keeping constant the total amount of rainfall in a growing season. The result is quite remarkable, due to the existence of two opposite mechanisms regulating the water balance. On one hand runoff production, for a given mean rainfall input, strongly depends on the ratio between soil depth and mean rainfall depth. The rapid decrease of runoff is thus somewhat analogous to that in the first part of Fig. 10(b), where a similar behavior was produced by an increase in soil depth. On the other hand interception increases almost linearly with λ. The interplay between these two mechanisms determines a maximum of both leakage and evapotranspiration at moderate values of λ (of course the position of the maxima changes according to the parameters used). This is particularly important from the vegetation point of view, since the mean transpiration rate is directly linked to productivity of ecosystems (e.g., [30, p. 383]). We have often pointed out in our discussion the importance not only of the amount, but also of the timing of rainfall in soil moisture dynamics, especially in water-controlled ecosystems (see also [46]). In this aspect the present figure seems to indicate the existence of an optimum for transpiration/productivity which is directly related to the climate-soil-vegetation characteristics. The particular position of this maximum in the parameter space is
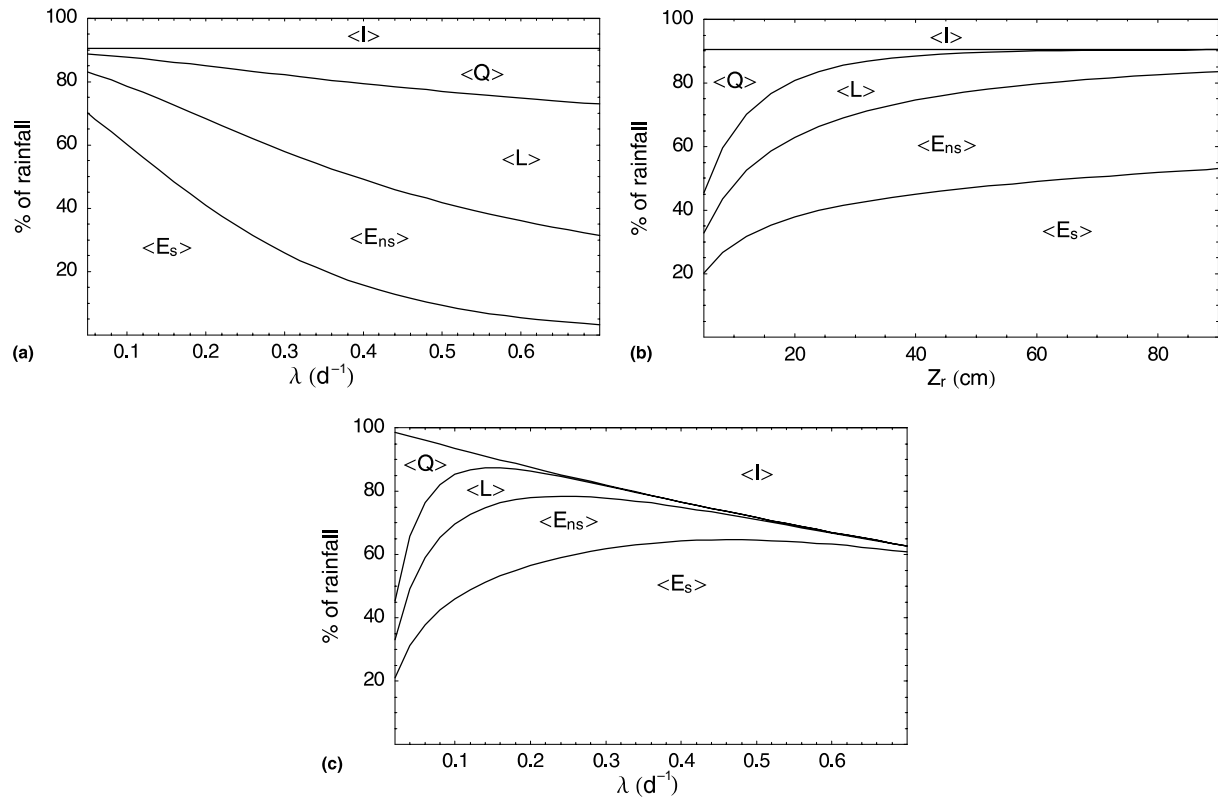
Fig. 10. Examples of the behavior of the components of the water balance normalized by the total rainfall. (a) Water balance as a function of the mean rainfall rate λ, for a shallow loamy soil ($Z_r = 30$ cm, $\alpha = 2$ cm). (b) Water balance as a function of the soil depth Z_r, for a loamy sand ($\alpha = 2$ cm, $\lambda = 0.2$ d^{-1}). (c) Water balance for a loamy sand as a function of the ratio between rainfall rate of occurrence (λ) and mean rainfall depth (α) for a constant mean total rainfall during a growing season, $\Theta = 60$ cm. Other common parameters are $E_w = 0.01$ cm/d, $E_{max} = 0.45$ cm/d, and $\Delta = 0.2$ cm (see Table 1 for soil parameters).

governed by the interplay of all the mechanisms acting in the soil–water balance, namely the intensity and amount of rainfall, interception, the active soil depth, and the nonlinear losses due to evapotranspiration and leakage.

5. Concluding remarks

The analytical solution of the stochastic model of soil water balance is illuminating in many issues, because it allows to have a quantitative comprehensive view of soil moisture dynamics and related phenomena. With the provision of not losing analytical tractability, we have tried nevertheless to make the model as realistic as possible. All the assumptions have been discussed in detail, especially the modeling of water losses, which is the point where the present analysis most differs from that of Rodriguez-Iturbe et al. [54].

The result is a model that provides general solutions that are in good agreement with physical expectations. Other investigations on soil moisture dynamics have used similar assumptions, concerning

both the stochastic representation of rainfall (e.g., [9,17,38]) and the behavior of losses due to evapotranspiration and leakage (e.g., [9,50]). In this concluding section, we discuss some recent field data which are considered important in regard to the model assumption presented in this paper.

The first set of information concerns the three-stage sequence of evapotranspiration losses from a shortgrass steppe, analyzed by Brutsaert and Chen ([5,6]; see also [52]). Using data sampled at a daily timescale, which is also the timescale adopted here, they reported the existence of three phases of drying with distinct temporal behavior. Such phases could correspond to the three different types of soil moisture control on evapotranspiration of the present model (e.g, Eq. (12)). According to their analysis, during the first stage of drying after an abundant rainfall, soil water evaporates both from the soil surface and from vegetation, at a rate which is governed by the available energy supply. This phase corresponds in our model to the range of soil moisture $\{s^*, 1\}$ or, according to Eq. (20) to the time interval $0 < t \leqslant t_s^*$. Then, after soil moisture content has decreased below a critical level, a transitional stage sets in, during which soil moisture is the controlling factor. This
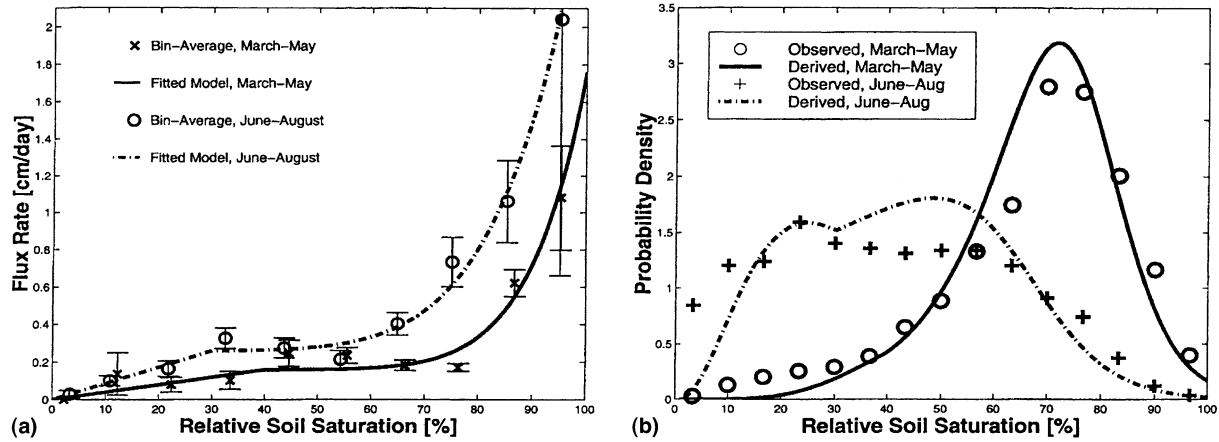
Fig. 11. (a) Estimation of water loss from conditional mean precipitation for a site in Illinois. (b) Observed and derived probability distributions of relative soil saturation (after [57]).

is in good agreement with the assumptions of our model where soil moisture controls transpiration through stomatal closure between s_w and s^*, or in the interval $t_{s^*} < t < t_{s_w}$. Finally, when soil moisture decreases below a certain threshold corresponding to grass wilting, drying takes place mainly as evaporation from the soil surface ($s_h < s \leqslant s_w$, or $t_{s_w} < t \leqslant \infty$). Brutsaert and Chen [5] refer to this phase as a desorption phase with a temporal decay proportional to $t^{-0.5}$, but they also maintain that different mathematical formulations could be possible for this phase. Moreover, the relevance of this last phase for modeling purposes is limited, except for extremely dry environments.

The second and most important experimental support to our model comes from the recent analysis by Salvucci [57]. He shows that for a stationary process the expected value of the change in soil moisture storage, conditioned on the storage s, is zero, so that the conditionally averaged net precipitation rate is equal to the moisture-dependent losses. Using averaged daily data of precipitation and soil moisture from a site in Illinois, and dividing the sample in two parts, one relative to the early growing season and the other to the late growing season, Salvucci [57] computed the conditionally averaged precipitation rate for various values of soil moisture. In this way he obtained soil moisture loss functions whose functional form closely agrees with the one used here, namely Eq. (16). Fig. 11(a) reproduces the loss functions obtained by Salvucci [57]. Employing such estimated loss functions, along with the estimates of the frequency of occurrence and mean depth of daily rainfall, λ and α, Salvucci [57] also computed the relative soil moisture pdfs with Eq. (25), obtaining an excellent match with the observed frequency distributions (Fig. 11(b)).

The model of soil moisture evolution presented in this paper provides a useful framework to investigate analytically the probabilistic structure of soil moisture and water balance. It allows to study, in a realistic way, the role of active soil depth and soil texture, the effect of plant physiological characteristics, and the importance of climatic parameters, as well as that of the timing and amount of rainfall in the dynamics of the soil moisture process. The same stochastic model of soil moisture will be employed in Part III [51] and Part IV [32] to investigate the temporal dynamics of vegetation water stress.

Acknowledgements

Appendix A. Soil moisture cumulative density function

The analytical expressions of the cumulative density function $P(s)$ of soil moisture and of the integration constant C of Eq. (31) are calculated in this section. The parameters used here are those defined in Eqs. (17)–(19). The expression is split in four parts resulting from the piecewise loss function (16). The $P(s)$ is obtained by direct integration of the pdf of soil moisture given by Eq. (31).

For $s_h < s \leqslant s_w$ the cumulative density function is

$$P(s) = \frac{C}{\eta_w} e^{-\gamma s_h} (s_w - s_h) [\gamma(s_w - s_h)]^{-\frac{\lambda'(s_w - s_h)}{\eta_w}}$$

$$\times \left\{ \Gamma \left[\frac{\lambda'(s_w - s_h)}{\eta_w} \right] - \Gamma \left[\frac{\lambda'(s_w - s_h)}{\eta_w}, \gamma(s - s_h) \right] \right\},$$

$$(A.1)$$

where $\Gamma[\cdot]$ and $\Gamma[\cdot,\cdot]$ are the complete and incomplete Gamma Function, respectively ([1], n. 6.1.1 and n. 6.5.3). For $s_w < s \leqslant s^*$ the $P(s)$ takes the form

$$P(s) = P(s_w) + \frac{C}{\eta - \eta_w}(s^* - s_w)\left[\frac{\eta_w\gamma(s^* - s_w)}{\eta - \eta_w}\right]^{-\gamma'\frac{s^* - s_w}{\eta - \eta_w}}$$

$$\times \exp\left(-\gamma\left(s_w - \frac{\eta_w(s^* - s_w)}{\eta - \eta_w}\right)\right)$$

$$\times \left\{\Gamma\left[\lambda'\frac{s^* - s_w}{\eta - \eta_w}, \frac{\eta_w\gamma(s^* - s_w)}{\eta - \eta_w}\right]\right.$$

$$\left. - \Gamma\left[\lambda'\frac{s^* - s_w}{\eta - \eta_w}, \gamma(s - s_w) + \frac{\eta_w\gamma(s^* - s_w)}{\eta - \eta_w}\right]\right\},$$

$$(A.2)$$

where $P(s_w)$ is the value of the cdf calculated in $s = s_w$ from Eq. (A.1). When $s^* < s \leqslant s_{fc}$ the cumulative density function is

$$P(s) = P(s^*) + \frac{C}{\lambda' - \gamma\eta}\left(\frac{\eta}{\eta_w}\right)^{\lambda'\frac{s^* - s_w}{\eta - \eta_w}}$$

$$\times \left[\exp\left(-\lambda s + \frac{\lambda'}{\eta}(s - s^*)\right) - e^{-\lambda s^*}\right] \qquad (A.3)$$

with the value of $P(s^*)$ calculated from Eq. (A.2). Finally, for $s_{fc} < s \leqslant 1$ the $P(s)$ can be written as

$$P(s) = P(s_{fc}) + \frac{C}{\gamma(\eta - m) - \lambda'}\left(\frac{\eta}{\eta_w}\right)^{\lambda'\frac{s^* - s_w}{\eta - \eta_w}}e^{\frac{\lambda'}{\eta}(s_{fc} - s^*)}$$

$$\times \left\{e^{-\gamma s_{fc}}\left(\frac{\eta}{\eta - m}\right)^{\frac{\lambda'}{\beta(\eta - m)}}{}_2F_1\left[\frac{\lambda'}{\beta(\eta - m)} + 1,\right.\right.$$

$$\times \frac{\lambda'}{\beta(\eta - m)} - \frac{\gamma}{\beta}; \frac{\lambda'}{\beta(\eta - m)} + 1 - \frac{\gamma}{\beta}; \frac{m}{m - \eta}\right]$$

$$- e^{-\gamma s}\left[\left(\frac{\eta}{\eta - m}\right)\left(\frac{e^{\beta(s - s_{fc})}m + \eta - m}{e^{-beta(s - s_{fc})}(\eta - m) + m}\right)\right]^{\frac{\lambda'}{\beta(\eta - m)}}$$

$$\times {}_2F_1\left[\frac{\lambda'}{\beta(\eta - m)} + 1, \frac{\lambda'}{\beta(\eta - m)} - \frac{\gamma}{\beta}; \frac{\lambda'}{\beta(\eta - m)}\right.$$

$$\left.\left.+ 1 - \frac{\gamma}{\beta}; \frac{e^{\beta s - s_{fc}}m}{m - \eta}\right]\right\}, \qquad (A.4)$$

where $P(s_{fc})$ is calculated from Eq. (A.3) and ${}_2F_1[\cdot,\cdot;\cdot,\cdot]$ is the Hypergeometric Function ([1], n. 15.1.1).

The integration constant C in Eqs. (A.1)–(A.4) is the same of Eq. (31). The analytical expression of C can be derived by imposing the condition $P(1) = 1$ in Eq. (A.4), and noticing that $P(s_{fc})$ in Eq. (A.4) is a function of C as well.

References

[1] Abramowitz M, Stegun IA. Handbook of mathematical functions. New York: Dover; 1964.

[2] Archer S, Scifres C, Bassham CR, Maggio R. Autogenic succession in a subtropical savanna: conversion of grassland to thorn woodland. Ecol Monogr 1988;58:90–102.

[3] Benjamin JR, Cornell CA. Probability, statistics, and decision for civil engineers. New York: McGraw-Hill; 1970.

[4] Brutsaert W. Evaporation into the atmosphere: theory, history, and applications. Dordrecht: D. Reidel Publishing Company; 1982.

[5] Brutsaert W, Chen D. Desorption and the two stages of drying of natural tallgrass prairie. Water Resour Res 1995;31(5):1305–13.

[6] Brutsaert W, Chen D. Diurnal variation of surface fluxes during thorough drying (or severe drought) of natural prairie. Water Resour Res 1996;32(7):2013–9.

[7] Canadell J, Jackson RB, Ehleringer JR, Mooney HA, Sala O, Schulze ED. Maximum rooting depth of vegetation types at the global scale. Oecologia 1996;108:583–95.

[8] Clapp RB, Hornberger GN. Empirical equations for some soil hydraulic properties. Water Resour Res 1978;14(8):601–4.

[9] Cordoba JR, Bras RL. Physically based probabilistic models of infiltration, soil moisture, and actual evapotranspiration. Water Resour Res 1981;17(1):93–106.

[10] Cosby BJ, Hornberger RB, Clapp RB, Ginn TR. A statistical exploration of the relationships of soil moisture characteristics to the physical properties of soils. Water Resour Res 1984;20(6):682–90.

[11] Cowan IR. Transport of water in the soil–plant–atmosphere system. J Appl Ecol 1965;2:221–39.

[12] Cox DR, Isham V. The virtual waiting-time and related processes. Adv Appl Prob 1986;18:558–73.

[13] Cox DR, Miller HD. The theory of stochastic processes. London: Methuen; 1965.

[14] Davidson JM, Nielsen DR, Biggar JW. The measurement and description of water flow through Columbia silt loam and Hisperia silt loam. Hilgardia 1963;34:601–16.

[15] De Wiest JM. Flow through porous media. New York: Academic Press; 1969.

[16] Dingman SL. Physical hydrology. Englewood Cliffs, NJ: Prentice-Hall; 1994.

[17] Eagleson PS. Climate, soil, and vegetation. 1. Introduction to water balance dynamics. Water Resour Res 1978;14(5):705–12.

[18] Eagleson PS, Segarra RI. Water-limited equilibrium of savanna vegetation systems. Water Resour Res 1985;21(10):1483–93.

[19] Feddes RA. Water, heat and crop growth. Wageningen, The Netherlands: Mededelingen; 1971. p. 57–72.

[20] Federer CA. A soil–plant–atmosphere model for transpiration and availability of soil water. Water Resour Res 1979;15(3):555–61.

[21] Federer CA. Transpiration supply and demand: plant, soil, and atmospheric effects evaluated by simulation. Water Resour Res 1982;18(2):355–62.

[22] Gardner WR, Ehlig CF. The influence of soil water on transpiration by plants. J Geophys Res 1963;68(20):5719–24.

[23] Gollan T, Turner NC, Schulze D. The responses of stomata and leaf gas exchange to vapour pressure deficit and soil water content, III. In the schlerophyllous woody species *Nerium oleander*. Oecologia 1985;65:356–62.

[24] Golluscio RA, Sala OE, Lauenroth WK. Differential use of large summer rainfall events by shrub and grasses: a manipulative experiment in the Patagonian steppe. Oecologia 1998;115:17–25.

[25] Hale MG, Orcutt DM. The physiology of plants under stress. New York: Wiley; 1987.

[26] Harr ME. Groundwater and seepage. New York: McGraw-Hill; 1962.

[27] Hillel D. Environmental soil physics. San Diego: Academic Press; 1998.

[28] Jackson RB, Canadell J, Ehleringer JR, Mooney HA, Sala O, Schulze D. A global analysis of root distribution for terrestrial biomes. Oecologia 1996;108:389–411.

[29] Jones HG. Plants and microclimate a quantitative approach to environmental plant physiology. 2nd ed. Cambridge, UK: Cambridge University Press; 1992.

[30] Kramer PJ, Boyer JS. Water relations of plants and soils. San Diego: Academic Press; 1995.

[31] Lai CT, Katul G. The dynamics role of root-water uptake in coupling potential to actual transpiration. Adv Water Res 2000;23:427–39.

[32] Laio F, Porporato A, Fernandez-Illescas CP. Rodriguez-Iturbe I. Plants in water-controlled ecosystems: active role in hydrological processes and response to water stress IV. Discussion of real cases. Adv Water Res 2001;24(7):745–62.

[33] Lange OL, Kappen L, Schulze D. Water and plant life: problems and modern approaches. Berlin: Springer; 1976.

[34] Larcher W. Physiological plant ecology. 3rd ed. Berlin: Springer; 1995.

[35] Ludlow MM. Ecophysiology of C_4 grasses. In: Lange OL, Kappen L, Schulze D, editors. Water and plant life. New York: Springer; 1976. p. 364–80.

[36] MacMahon JA, Schimpf DJ. Water as a factor in the biology of North American plants. In: Evans DD, Thames JL, Stroudburg Pa, editors. Water in desert ecosystems. USA: Dowden, Hutchinson Ross; 1981.

[37] Major JA. Climatic index to vascular plant activity. Ecology 1963;44(3):485–98.

[38] Milly PCD. An analytic solution of the stochastic storage problem applicable to soil water. Water Resour Res 1993; 29(11):3755–8.

[39] Milly PCD. Sensitivity of greenhouse summer dryness to changes in plant rooting characteristics. Geophys Res Lett 1997;24(2):269–71.

[40] Milly PCD, Dunne KA. Sensitivity of the global water cycle to the waterholding capacity of land. J Climate 1993;7:508–26.

[41] Naveh Z. Mediterranean cosystems and vegetation types in California and Israel. Ecology 1967;48(3):445–59.

[42] Nepstad DC, de Carvalho CR, Davidson A, Jipp PH, Levebvre PA, Negreiros GH, et al. The role of deep roots in the hydrological and carbon cycle of Amazonian forests and pastures. Nature 1994;372:666–9.

[43] Ng E, Miller PC. Soil moisture relations in the Southern California Caparral. Ecology 1980;61(1):98–107.

[44] Nilsen T, Orcutt DM. Physiology of plants under stress: abiotic factors. New York: Wiley; 1998.

[45] Nobel PS. Physicochemical and environmental plant physiology. 2nd ed. San Diego: Academic Press; 1999.

[46] Noy-Meir I. Desert ecosystems: environment and producers. Ann Rev Ecol Syst 1973;4:25–51.

[47] Oertli JJ. The soil–plant–atmosphere continuum. In: Lange OL, Kappen L, Schulze D, editors. Water and plant life. New York: Springer; 1976. p. 34–41.

[48] Parlange MB, Katul GG, Folegatti MV, Nielsen DR. Evaporation and the field scale diffusivity function. Water Resour Res 1993;29(4):1279–86.

[49] Parlange MB, Eichinger W, Albertson JD. Regional scale evaporation and the atmospheric boundary layer. Rev Geophys 1995;33(1):99–124.

[50] Paruelo JM, Sala O. Water losses in the Patagonian steppe: a modeling approach. Ecology 1995;76(2):510–20.

[51] Porporato A, Laio F, Ridolfi L, Rodriguez-Iturbe I. Plants in water-controlled ecosystems: active role in hydrological processes and response to water stress III. Vegetation water stress. Adv Water Res 2001;24(7):725–44.

[52] Porte-Agel F, Parlange MB, Cahill AT, Gruber A. Mixture of time scales in land-atmosphere interaction: desorption and self-similarity of energy fluxes. Agron J 2000;92(5):832–6.

[53] Richter H. The water status in plant-experimental evidence. In: Lange OL, Kappen L, Schulze D, editors. Water and plant life. NewYork: Springer; 1976. p. 42–55.

[54] Rodriguez-Iturbe I, Porporato A, Ridolfi L, Isham V, Cox D. Probabilistic modelling of water balance at a point:the role of climate, soil and vegetation. Proc R Soc Lond A 1999;455:3789–805.

[55] Rodriguez-Iturbe I, Porporato A, Laio F, Ridolfi L. Plants in water-controlled ecosystems: active role in hydrological processes and response to water stress I. Scope and general outline. Adv Water Res 2001;24(7):695–705.

[56] Sala O, Lauenroth WK, Parton WJ. Long-term soil water dynamics in the shortgrass steppe. Ecology 1992;73(4):1175–81.

[57] Salvucci GD. Estimating the moisture dependence of root-zone water loss using conditionally averaged precipitation. Water Resour Res, to appear.

[58] Sarmiento G. The ecology of neotropical savannas, translated by Solbrig O. Cambridge, MA: Harvard University Press; 1984.

[59] Scholes RJ, Archer SR. Tree–grass interactions in savannas. Ann Rev Ecol Syst 1997;28:517–44.

[60] Scholes RJ, Walker BH. An African savanna. Cambridge, UK: Cambridge University Press; 1993.

[61] Schulze D. Carbon dioxide and water vapor exchange in response to drought in the atmosphere and in the soil. Ann Rev Plant Physiol 1986;37:247–74.

[62] Schulze D. Soil water deficits and atmospheric humidity as environmental signals. In: Smith JAC, Griffiths H, editors. Water deficits: plant response from cell to community. Oxford, UK: Bios Scientific Publishers; 1993.

[63] Schulze D, Mooney HA, Sala OE, Jobbagy E, Buchmann N, Bauer G, et al. Rooting depth, water availability, and vegetation cover along an aridity gradient in Patagonia. Oecologia 1996;108:503–11.

[64] Sisson JB, Klittich WM, Salem SB. Comparison of two methods for summarizing hydraulic conductivities of layered soil. Water Resour Res 1988;24(8):1271–6.

[65] Slatyer RO. Plant water relationships. London: Academic Press; 1967.

[66] Smith JAC, Griffith H. Water deficits: plant responses from cell to community. Oxford, UK: Bios Scientific Publishers; 1993.

[67] Spittlehouse DL, Black TA. A growing season water balance model applied to two Douglas fir stands. Water Resour Res 1981;17(6):1651–6.

[68] Waring RH, Running SW. Forest cosystems:analysis at multiple scales. 2nd ed. San Diego: Academic Press; 1998.